



# Desorption dynamics of CO<sub>2</sub> from formate decomposition on Cu(111)<sup>†</sup>

Fahdzi Muttaqien,<sup>a</sup> Hiroyuki Oshima,<sup>a</sup> Yuji Hamamoto,<sup>ab</sup> Kouji Inagaki,<sup>ab</sup>  
Ikutaro Hamada<sup>b</sup> and Yoshitada Morikawa<sup>abc</sup>

Cite this: *Chem. Commun.*, 2017, 53, 9222

Received 15th May 2017,  
Accepted 22nd July 2017

DOI: 10.1039/c7cc03707d

rsc.li/chemcomm

We performed *ab initio* molecular dynamics analysis of formate decomposition to CO<sub>2</sub> and H on a Cu(111) surface using van der Waals density functionals. Our analysis shows that the desorbed CO<sub>2</sub> has approximately twice larger bending vibrational energy than the translational, rotational, and stretching vibrational energies. Since formate synthesis, the reverse reaction of formate decomposition, has been suggested experimentally to occur via the Eley–Rideal mechanism, our results indicate that the formate synthesis can be enhanced if the bending vibrational mode of CO<sub>2</sub> is excited rather than the translational and/or stretching vibrational modes. Detailed information on the energy distribution of desorbed CO<sub>2</sub> as a formate decomposition product may provide new insights for improving the catalytic activity of formate synthesis.

One of the most important intermediate steps in the methanol synthesis over Cu-based catalysts is CO<sub>2</sub> hydrogenation into formate (HCOO).<sup>1–5</sup> Based on a kinetics analysis, it was clarified that formate synthesis is structure insensitive and consistent with an Eley–Rideal (ER) type mechanism.<sup>6–9</sup> Recently, theoretical investigations also suggested the ER and hot atom (HA) mechanisms during CO<sub>2</sub> reduction into formate and/or hydrocarboxyl (HOCO).<sup>10</sup> The ER type mechanism suggests that the formate synthesis can be enhanced by controlling the translational, vibrational, and rotational energies of impinging CO<sub>2</sub>. The initial impinging CO<sub>2</sub> energies must be related to the energy states of desorbed CO<sub>2</sub> from formate decomposition because formate synthesis and decomposition are reverse reactions. Therefore, the elucidation of formate decomposition dynamics is important for improving catalytic formate synthesis.

Very recently, the dynamics of desorbed CO<sub>2</sub> produced from the formate decomposition reaction has been studied by measuring the angle-resolved intensity and translational energy distribution of the steady-state reaction of formic acid (HCOOH) and oxygen on a Cu surface.<sup>11</sup> It was reported that the translational energy of desorbed CO<sub>2</sub> is approximately 0.10 eV and independent of the surface temperature. The measured CO<sub>2</sub> translational energy is much smaller than the activation energy of formate synthesis, which is 0.59 ± 0.05 eV.<sup>7–9</sup> This suggests that internal modes, such as vibrational and rotational modes, should be excited in the desorbed CO<sub>2</sub>. In this study, we therefore investigate the energy distribution of desorbed CO<sub>2</sub> as a formate decomposition product by means of *ab initio* calculations. We also show the importance of the van der Waals (vdW) interaction in determining the energetics of desorbed CO<sub>2</sub>. From the knowledge of desorbing product dynamics, we can deduce optimal conditions for the formate synthesis reaction through CO<sub>2</sub> hydrogenation.

The calculations were performed using a plane-wave pseudo-potential code named “Simulation tool for Atom TEchnology (STATE)”.<sup>12</sup> Since the vdW interaction is important to describe the adsorption and chemical reaction of inert molecules,<sup>13</sup> we compare the Perdew–Burke–Ernzerhof (PBE) results with those obtained using vdW density functionals (vdW-DFs), *i.e.*, the original vdW-DF (vdW-DF1),<sup>14</sup> optB86b-vdW,<sup>15</sup> and rev-vdW-DF2<sup>16</sup> functionals as implemented in the STATE code.<sup>17</sup> We also included the dispersion correction proposed by Grimme with PBE (PBE-D2).<sup>18</sup> We performed *ab initio* molecular dynamics (AIMD) simulations starting from the transition state (TS) structure of the formate decomposition process to gas phase CO<sub>2</sub> and adsorbed H to evaluate the translational and internal (rotational and vibrational) energies of desorbed CO<sub>2</sub>. We have also considered additional samples of the initial geometry for AIMD simulations. We displaced the atoms at the TS towards the second, third, fourth, fifth, and sixth lowest normal mode vectors in such a way that the energies of the displaced geometries are increased from the energy of the TS by 0.02 eV. In the AIMD simulations, the initial

<sup>a</sup> Department of Precision Science and Technology, Graduate School of Engineering, Osaka University, 2-1, Yamada-oka, Suita, Osaka 565-0871, Japan.

E-mail: fahdzi@cp.prec.eng.osaka-u.ac.jp, morikawa@prec.eng.osaka-u.ac.jp

<sup>b</sup> Elements Strategy Initiative for Catalysts and Batteries (ESICB), Kyoto University, Katsura, Kyoto 615-8520, Japan

<sup>c</sup> Research Center for Ultra-Precision Science and Technology, Graduate School of Engineering, Osaka University, Japan

<sup>†</sup> Electronic supplementary information (ESI) available: Additional information. See DOI: 10.1039/c7cc03707d



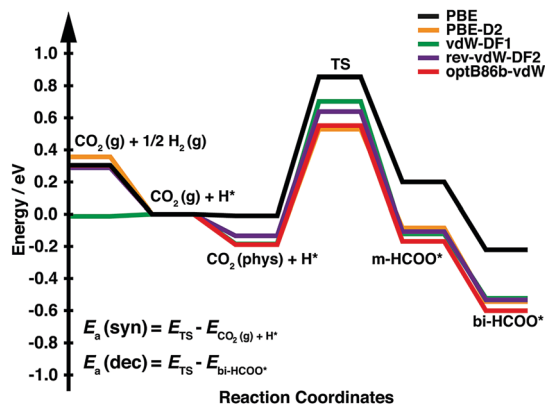


Fig. 1 Energy profile for CO<sub>2</sub> hydrogenation to bidentate formate on Cu(111). The energy zero is the sum of the total energies of gas phase CO<sub>2</sub> and an adsorbed hydrogen on the surface (CO<sub>2</sub>(g) + H\*).

velocities are given randomly and they are scaled to set the average kinetic energy of 300 K. Here, we do not include the zero-point energy in the sampling of initial conditions. The detailed calculation methods are provided in the ESI.†

We first calculated the minimum energy path of CO<sub>2</sub> hydrogenation into bidentate formate (bi-HCOO) through monodentate formate (m-HCOO) on Cu(111). The bidentate formate has been observed experimentally as an abundant product during CO<sub>2</sub> hydrogenation compared with its isomer (hydrocarboxyl (HOCO)).<sup>7–9</sup> Moreover, we have also performed the calculations of HOCO adsorption on Cu(111) and found that this species is 0.89 eV less stable using one of the vdW-DFs (optB86b-vdW). Fig. 1 and Table 1 show the energy profile of CO<sub>2</sub> hydrogenation into formate and its detailed descriptions, respectively. As shown in Fig. 1, the hydrogen chemisorption energies (the energy levels of CO<sub>2</sub>(g) + 1/2H<sub>2</sub>(g)) are quite similar among all functionals except vdW-DF1. On the other hand, the physisorption energies of CO<sub>2</sub> (the energy levels of CO<sub>2</sub>(phs) + H\*), the energies of the TSs, m-HCOO\*, and bi-HCOO\* are stabilized through the vdW attraction by approximately 0.13–0.37 eV relative to the PBE result. We then consider the activation energy of formate synthesis ( $E_a(\text{syn})$ ) as the

energy difference between the TS and the CO<sub>2</sub>(g) + H\* state. This definition of  $E_a(\text{syn})$  should correspond to the experimentally observed activation energy of formate synthesis, in which formate was synthesized at a temperature of 333–353 K under atmospheric pressure.<sup>7</sup> Under these conditions, the hydrogen coverage is close to the saturation point, while CO<sub>2</sub> coverage is almost negligible due to a small adsorption energy. The activation energy of formate decomposition ( $E_a(\text{dec})$ ) is defined as the energy difference between the TS and bi-HCOO\*. As shown in Table 1, only PBE overestimates the experimental  $E_a(\text{syn})$ , while each functional with a vdW interaction gives a reasonably good result. Meanwhile, each calculated  $E_a(\text{dec})$  is in good agreement with the experimental results.

Next, we explored the energy distribution of desorbed CO<sub>2</sub> as a product of formate decomposition. We calculated the CO<sub>2</sub> translational energy ( $E_t$ ) from the velocity of the center of mass of CO<sub>2</sub>. Fig. 2a summarizes the time evolution of CO<sub>2</sub> translational energy. The representative snapshots of CO<sub>2</sub> desorption from the AIMD trajectory are shown in Fig. 2b. There are significant differences in the  $E_t$  profiles calculated using PBE and those using PBE-D2 and vdW-DFs. Here, PBE predicts a constant  $E_t$  value at 0.30 eV after the CO<sub>2</sub> molecule experiences Pauli repulsion in the first 0.10 ps (shown as a black line in Fig. 2a). Meanwhile, the PBE-D2 and vdW-DFs show different time evolution profiles of the CO<sub>2</sub> translational energy. In the first 0.08–0.10 ps, the  $E_t$  value increases to 0.20–0.32 eV due to the Pauli repulsion between CO<sub>2</sub> and the surface. Then, it decreases gradually to a certain value. The decrease in the CO<sub>2</sub> translational energy is due to the vdW attraction between CO<sub>2</sub> and the Cu(111) surface. We also estimated the desorption angle ( $\beta$ ) of CO<sub>2</sub> at 0.68 ps, when it already has a constant  $E_t$  value, from the direction of the velocity of center of mass relative to the surface normal (Fig. 2b). The calculated  $\beta$  using PBE, PBE-D2, vdW-DF1, rev-vdW-DF2, and optB86b-vdW are 5°, 18°, 8°, 12°, and 14°, respectively, in which the angular distribution of desorbed CO<sub>2</sub> shows quite sharp collimation along the surface normal direction and is in good agreement with the experimental results.<sup>11</sup> As summarized in Table 2, the calculated  $E_t$  values using PBE-D2 and vdW-DFs are in reasonable

Table 1 Detailed descriptions of the energy profile of CO<sub>2</sub> hydrogenation into formate (in eV) on Cu(111), and calculated formate synthesis and decomposition energies using PBE, PBE-D2, and vdW-DFs. The values in brackets were obtained using a six layer-thick slab. The zero-point energy (ZPE) correction is evaluated using the optB86b-vdW functional

	This study					Expt.
	PBE	PBE-D2	vdW-DF1	rev-vdW-DF2	optB86b-vdW	
$E_{\text{CO}_2(\text{g}) + 1/2\text{H}_2(\text{g})}$	+0.30 (+0.22)	+0.36	−0.01	+0.29	+0.30 (+0.22)	—
$E_{\text{CO}_2(\text{phs}) + \text{H}^*}$	−0.01 (−0.01)	−0.19	−0.18	−0.13	−0.19 (−0.18)	—
$E_{\text{TS}}$	+0.85 (+0.78)	+0.53	+0.70	+0.64	+0.55 (+0.52)	—
$E_{\text{m-HCOO}^*}$	+0.20 (+0.17)	−0.08	−0.12	−0.11	−0.17 (−0.18)	—
$E_{\text{bi-HCOO}^*}$	−0.22 (−0.33)	−0.54	−0.52	−0.53	−0.60 (−0.70)	—
$E_a(\text{syn})$	0.85 (0.78)	0.53	0.70	0.64	0.55 (0.52)	—
$E_a(\text{syn}) + \text{ZPE}$	0.80 (0.73)	0.48	0.65	0.59	0.50 (0.47)	0.59 ± 0.05 <sup>a</sup> 0.66 ± 0.02 <sup>b</sup>
$E_a(\text{dec})$	1.08 (1.12)	1.07	1.23	1.17	1.15 (1.22)	—
$E_a(\text{dec}) + \text{ZPE}$	0.90 (0.94)	0.89	1.05	0.99	0.97 (1.04)	1.12 ± 0.03 <sup>a</sup> 1.17 ± 0.13 <sup>b</sup>

<sup>a</sup> Taken from ref. 7. <sup>b</sup> Taken from ref. 8 and 9.



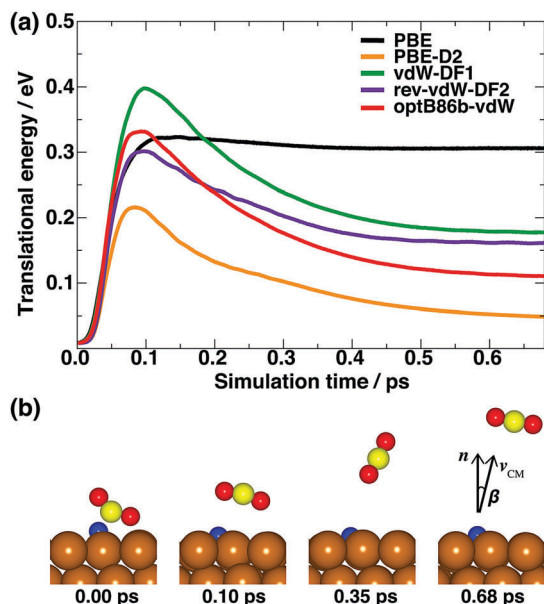


Fig. 2 (a) Time evolution of the translational energy of desorbed CO<sub>2</sub> from formate decomposition calculated using PBE, PBE-D2, and vdW-DFs. (b) Representative snapshots from the AIMD trajectory of CO<sub>2</sub> desorption.  $\hat{n}$  and  $v_{CM}$  represent the direction of the surface normal and the velocity of the center of mass of CO<sub>2</sub>, respectively.

agreement with the experimental estimation,<sup>11</sup> while PBE fails in predicting this energy. Therefore, the vdW interaction is important for describing the translational energy of desorbed CO<sub>2</sub>.

We also evaluated the energy transfer by formate decomposition into the internal modes (rotational and vibrational) of CO<sub>2</sub>. The rotational energy ( $E_r$ ) of CO<sub>2</sub> as a function of time was calculated from the moment of inertia of CO<sub>2</sub> and its angular momentum at each time step of the MD trajectory. Table 2 shows that the calculated  $E_r$  value varies in between 0.08 and 0.11 eV. The CO<sub>2</sub> bending, symmetric stretching, antisymmetric stretching vibrational energies are evaluated based on the time evolution of the desorbed CO<sub>2</sub> geometry, *i.e.*, bond angle ( $\theta$ ), the C–O bond length ( $l$ ), and the difference between two C–O bond lengths ( $\Delta$ ), respectively, as shown in Fig. 3. For comparison, we also

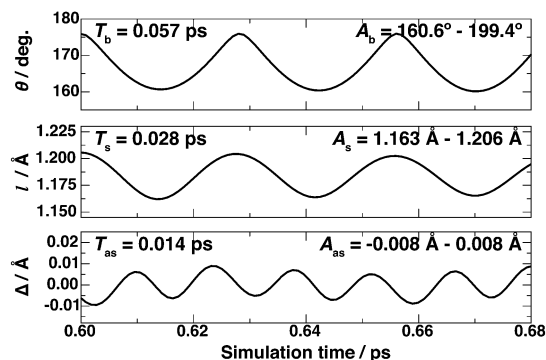


Fig. 3 Time evolution of the CO<sub>2</sub> bond angle ( $\theta$ ), the C–O bond length ( $l$ ), and the difference between two C–O bond lengths ( $\Delta$ ) based on the AIMD trajectory calculated using the optB86b-vdW functional. The period ( $T$ ) and amplitude ( $A$ ) of each geometry data are shown in each panel.

evaluated the vibrational frequencies of an isolated CO<sub>2</sub> (see the ESI†). The calculated zero-point energies of isolated CO<sub>2</sub> bending, symmetric stretching, and antisymmetric stretching vibrational modes using optB86b-vdW are 76.72 meV, 164.61 meV, and 295.74 meV, respectively, which are in good agreement with the experimental values of 82.70 meV, 165.27 meV, and 291.24 meV, respectively.<sup>19,20</sup> These calculated zero-point energies are nearly independent of the functional. The vibrational energy of the bending mode ( $E_b \sim 0.25$  eV) of desorbed CO<sub>2</sub> is close to the third excitation of the zero-point energy of isolated CO<sub>2</sub>. All functionals produce similar  $E_b$  values in the range of 0.24–0.26 eV. The calculated vibrational energy of the CO<sub>2</sub> symmetric mode ( $E_s$ ) varies between 0.05 and 0.11 eV, which is close to the zero-point energy of the isolated CO<sub>2</sub> symmetric mode. Meanwhile, the vibrational energy of the antisymmetric mode ( $E_{as} \sim 1.5$  meV) is much smaller than the zero-point energy of isolated CO<sub>2</sub>.

Based on our calculations, nearly a half of  $E_a(\text{syn})$  is transferred into the CO<sub>2</sub> bending mode, a quarter into each translational and rotational modes, and rather a small energy is transferred into the CO<sub>2</sub> stretching modes. The origin for the strong enhancement of the CO<sub>2</sub> bending mode can be ascribed to its geometry at the TS, in which the CO<sub>2</sub> bond angle is nearly 140°. The rest of  $E_a(\text{syn})$  may have transferred into the surface modes, namely, hydrogen–Cu and/or Cu–Cu vibrations. We also performed the sudden vector projection (SVP) analysis proposed by Jiang and Guo.<sup>21</sup> We showed that the SVP analysis qualitatively agrees rather well with our AIMD simulation results (shown in the ESI†). Therefore, our results strongly suggest that formate synthesis, the reverse process of the formate decomposition, can be enhanced by increasing the vibrational energy of the CO<sub>2</sub> bending mode.

The present results are in sharp contrast to the case of CO<sub>2</sub> dissociation, in which the CO<sub>2</sub> symmetric and antisymmetric stretching modes are theoretically suggested to be more important to increase the dissociation rate.<sup>22</sup> The importance of stretching modes in the CO<sub>2</sub> dissociation was implied experimentally in the study of CO<sub>2</sub> dynamics from CO oxidation on Pd surfaces.<sup>23–25</sup> The desorbed CO<sub>2</sub> has 0.12–0.16 eV in the vibrational energy of the antisymmetric mode, which is slightly

**Table 2** Calculated translational energy ( $E_t$ ), rotational energy ( $E_r$ ), vibrational energy of the bending mode ( $E_b$ ), and vibrational energy of the symmetric stretching mode ( $E_s$ ) of desorbed CO<sub>2</sub> from formate decomposition on Cu(111) using PBE, PBE-D2, and vdW-DFs (in eV). The calculation results using the optB86b-vdW functional are the average results from several samples of AIMD trajectory

	This study					Expt. <sup>a</sup>
	PBE	PBE-D2	vdW-DF1	rev-vdW-DF2	optB86b-vdW	
$E_t$	0.30	0.05	0.18	0.16	0.14 ± 0.03	0.10
$E_r$	0.08	0.09	0.08	0.11	0.11 ± 0.03	—
$E_b$	0.27	0.24	0.25	0.26	0.26 ± 0.02	—
$E_s$	0.06	0.05	0.10	0.08	0.04 ± 0.02	—
Surface mode <sup>b</sup>	0.14	0.10	0.09	0.03	0.03 ± 0.02	—

<sup>a</sup> Experimentally measured CO<sub>2</sub> translational energy as a formate decomposition product taken from ref. 11. <sup>b</sup> This energy is deduced from:  $E_a(\text{syn}) - (E_t + E_r + E_b + E_s)$ .



larger than the vibrational energy of the CO<sub>2</sub> symmetric-bending mode (0.11–0.13 eV). Moreover, the measured translational (0.10–0.12 eV)<sup>26</sup> and rotational (0.08–0.10 eV)<sup>23,25,27,28</sup> energies of desorbed CO<sub>2</sub> from CO oxidation on Pd surfaces are smaller than its vibrational energy of the antisymmetric mode. Therefore, CO<sub>2</sub> dissociation can be selectively enhanced by exciting the CO<sub>2</sub> stretching vibrational modes.

Finally, we discuss the temperature dependence of the translational energy of CO<sub>2</sub>. Experimentally, it was reported that  $E_t$  of desorbed CO<sub>2</sub> from formate decomposition is independent of the surface temperature,<sup>11</sup> while that from CO oxidation is linearly dependent on the surface temperature.<sup>26</sup> From our theoretical simulations, it turns out that at most 20% of  $E_a(\text{syn})$  is transferred into surface modes. On the other hand, it can be deduced that approximately 60% of the activation energy of CO<sub>2</sub> dissociation (1.30 eV)<sup>29</sup> on a Pd surface, which is a reverse reaction of CO oxidation, is transferred to the surface mode. Both results, namely, the surface temperature dependence and the energy transfer to the surface mode, indicate the strength of the coupling between CO<sub>2</sub> and the surfaces at the TS of reactions. In the case of formate decomposition, CO<sub>2</sub> is weakly bonded as seen in the left panel of Fig. 2b. This is in contrast to the case of CO oxidation, where CO<sub>2</sub> was found to spend a significant residence time in the chemisorption well before it desorbs.<sup>30</sup> Moreover, one of the two C–O bond lengths of CO<sub>2</sub> is significantly elongated at the TS of CO oxidation, and carbon and oxygen are strongly bonded to the surface.<sup>31</sup>

In summary, we have investigated the minimum energy path of CO<sub>2</sub> hydrogenation into formate and the dynamics of formate decomposition into gas phase CO<sub>2</sub> and adsorbed hydrogen using density functional theory calculations. Based on the dynamics analysis of formate decomposition, the bending energy of desorbed CO<sub>2</sub> is twice larger than the translational energy. Since formate synthesis from CO<sub>2</sub> and H<sub>2</sub>, the reverse reaction of the formate decomposition, is experimentally suggested to occur *via* the ER type mechanism, our results indicate that the reaction rate of formate synthesis can be enhanced if the bending vibrational mode of CO<sub>2</sub> is excited rather than the translational and/or stretching modes. Meanwhile, these results are quite different from the case of CO<sub>2</sub> dissociation, in which the antisymmetric stretching mode is the key to increasing the dissociation rate. Accordingly, we anticipate that this work may contribute to the future development in controlling the particular molecular vibrational mode for improving catalytic reactions.

The authors thank Prof. Junji Nakamura, Prof. Takahiro Kondo, and Dr Jiamei Quan for their valuable discussions. The present work was supported by the Advanced Catalytic Transformation Program for Carbon utilization (ACT-C) (Grant No. JPMJCR12YU) of the Japan Science and Technology Agency (JST), and partly supported by Grants-in Aid for Scientific Research on Innovative Areas 3D Active-Site Science (No. 26105010 and No. 26105011) from the Japan Society for the Promotion of Science (JSPS) and the Elements Strategy Initiative for Catalysts and Batteries (ESICB) supported by the Ministry of

Education, Culture, Sports, Science, and Technology, Japan (MEXT). The numerical calculations were performed using the computer resources at the Institute for Solid State Physics (ISSP), Univ. of Tokyo, and the HPCI systems provided by Nagoya Univ., Univ. of Tokyo, and Tohoku Univ. through the HPCI System Research Project (Project ID: hp130112, hp140166, and hp150201).

## References

- 1 S. Kattel, P. J. Ramirez, J. G. Chen, J. A. Rodriguez and P. Liu, *Science*, 2017, **355**, 1296–1299.
- 2 S. Kuld, M. Thorhauge, H. Falsig, C. F. Elkjær, S. Helveg, I. Chorkendorff and J. Sehested, *Science*, 2016, **352**, 969–974.
- 3 M. Behrens, F. Stüttgen, I. Kasatkin, S. Köhl, M. Hävecker, F. Abild-Pedersen, S. Zander, F. Girgsdies, P. Kurr, B.-L. Knief, M. Tovar, R. W. Fischer, J. K. Nørskov and R. Schlögl, *Science*, 2012, **336**, 893–897.
- 4 L. C. Grabow and M. Mavrikakis, *ACS Catal.*, 2011, **1**, 365–384.
- 5 T. Fujitani, I. Nakamura, T. Uchijima and J. Nakamura, *Surf. Sci.*, 1997, **383**, 285–298.
- 6 G. Wang, Y. Morikawa, T. Matsumoto and J. Nakamura, *J. Phys. Chem. B*, 2006, **110**, 9–11.
- 7 H. Nakano, I. Nakamura, T. Fujitani and J. Nakamura, *J. Phys. Chem. B*, 2001, **105**, 1355–1365.
- 8 H. Nishimura, T. Yatsu, T. Fujitani, T. Uchijima and J. Nakamura, *J. Mol. Catal. A: Chem.*, 2000, **155**, 3–11.
- 9 I. Nakamura, H. Nakano, T. Fujitani, T. Uchijima and J. Nakamura, *J. Vac. Sci. Technol., A*, 1999, **17**, 1592–1595.
- 10 W. Lin, K. M. Stocker and G. C. Schatz, *J. Am. Chem. Soc.*, 2017, **139**, 4663–4666.
- 11 J. Quan, T. Kondo, G. Wang and J. Nakamura, *Angew. Chem., Int. Ed.*, 2017, **56**, 3496–3500.
- 12 Y. Morikawa, K. Iwata, J. Nakamura, T. Fujitani and K. Terakura, *Chem. Phys. Lett.*, 1999, **304**, 91–97.
- 13 F. Nattino, D. Migliorini, M. Bonfanti and G.-J. Kroes, *J. Chem. Phys.*, 2016, **144**, 044702.
- 14 M. Dion, H. Rydberg, E. Schröder, D. C. Langreth and B. I. Lundqvist, *Phys. Rev. Lett.*, 2004, **92**, 246401.
- 15 J. Klimeš, D. R. Bowler and A. Michaelides, *Phys. Rev. B: Condens. Matter Mater. Phys.*, 2011, **83**, 195131.
- 16 I. Hamada, *Phys. Rev. B: Condens. Matter Mater. Phys.*, 2014, **89**, 121103.
- 17 Y. Hamamoto, I. Hamada, K. Inagaki and Y. Morikawa, *Phys. Rev. B*, 2016, **93**, 245440.
- 18 S. Grimme, *J. Comput. Chem.*, 2006, **27**, 1787–1799.
- 19 T. Shimanouchi, *Tables of Molecular Vibrational Frequencies, Consolidated Volume 1*, National Standard Reference Data System (NSRDS), Tokyo, Japan, 1972.
- 20 W. B. Person and G. Zerbi, *Vibrational intensities in infrared and Raman spectroscopy*, Elsevier Scientific Pub. Co., Amsterdam, Netherlands, 1982.
- 21 B. Jiang and H. Guo, *J. Chem. Phys.*, 2013, **138**, 234104.
- 22 B. Jiang and H. Guo, *J. Chem. Phys.*, 2016, **144**, 091101.
- 23 T. Yamanaka, *Phys. Chem. Chem. Phys.*, 2008, **10**, 5429–5435.
- 24 K. Nakao, S. Ito, K. Tomishige and K. Kunimori, *Catal. Today*, 2006, **111**, 316–321.
- 25 K. Nakao, S. Ito, K. Tomishige and K. Kunimori, *J. Phys. Chem. B*, 2005, **109**, 17553–17559.
- 26 K. Kimura, Y. Ohno and T. Matsushima, *Surf. Sci.*, 1999, **429**, L455–L461.
- 27 H. Uetsuka, K. Watanabe, H. Ohnuma and K. Kunimori, *Surf. Sci.*, 1997, **377**, 765–769.
- 28 H. Uetsuka, K. Watanabe and K. Kunimori, *Surf. Sci.*, 1996, **363**, 73–78.
- 29 T. Engel and G. Ertl, *J. Chem. Phys.*, 1978, **69**, 1267–1281.
- 30 X. Zhou, B. Kolb, X. Luo, H. Guo and B. Jiang, *J. Phys. Chem. C*, 2017, **121**, 5594–5602.
- 31 A. Alavi, P. Hu, T. Deutsch, P. L. Silvestrelli and J. Hutter, *Phys. Rev. Lett.*, 1998, **80**, 3650–3653.

